1521-009X/46/11/1703–1711$35.00
Drug Metabolism and Disposition

https://doi.org/10.1124/dmd.118.082727
Drug Metab Dispos 46:1703–1711, November 2018

Special Section – New Models in Drug Metabolism and Transport

Human Pluripotent Stem Cell–Derived Kidney Model for Nephrotoxicity Studies[S]

Piyush Bajaj, A. David Rodrigues, Claire M. Steppan, Sandra J. Engle, Sumathy Mathialagan, and Thomas Schroeter

Discovery Sciences (P.B., C.M.S., S.J.E., T.S.) and Pharmacokinetics, Dynamics, and Metabolism (A.D.R., S.M.), Pfizer Worldwide Research and Development, Pfizer Inc., Groton, Connecticut

Received May 30, 2018; accepted August 28, 2018

ABSTRACT

Current in vitro models for identifying nephrotoxins are poorly predictive. We differentiated human pluripotent stem cells (hPSCs) into three-dimensional, multicellular structures containing proximal tubule cells (PTCs) and podocytes and evaluated them as a platform for predicting nephrotoxicity. The PTCs showed megalin-dependent, cubilin-mediated endocytosis of fluorescently labeled dextran and active gamma-glutamyl transpeptidase enzymes. Transporters from both the ATP-binding cassette (ABC) and the solute carrier (SLC) families were present at physiological levels in the differentiated cells, but important renal transporters such as organic anion transporter 1 (OAT1), OAT3, and organic cation transporter 2 (OCT2) were present only at lower levels. Radioactive uptake studies confirmed the functional activity of organic cation transporter, novel, type 2 (OCTN2), organic anion transporter polypeptide 4C1 (OATP4C1), and OCTs/multidrug and toxin extrusion proteins (MATEs). When treated with 10 pharmacologic agents as a test of the platform, the known nephrotoxic compounds were distinguished from the more benign compounds by an increase in tubular (PTC, kidney injury molecule 1 (KIM-1), and heme oxygenase 1 (HO-1)) and glomerular (nephrin [NPHS1]/Wilms tumor protein [WT1]) markers associated with nephrotoxicity, and we were able to distinguish the type of nephrotoxin by examining the relative levels of these markers. Given the functions demonstrated and with improved expression of key renal transporters, this hPSC-derived in vitro kidney model shows promise as a platform for detection of mechanistically different nephrotoxins.

Introduction

The kidney is a key organ involved in the elimination of drugs from the circulation. Approximately 32% of the top 200 drugs are cleared by the kidney (Morrissey et al., 2013). The current models used to predict nephrotoxicity are insufficient because nephrotoxicity causes only 2% of compound attrition in preclinical studies but 19% of the attrition in phase III clinical trials (Bonventre et al., 2010; Jang et al., 2013). Animal models have shown limited predictive value, and human in vitro models of kidney function have been challenging to develop because the nephron, the functional filtering unit of the kidney, is composed of several different cell types with specific interactions, architecture, and dynamic microenvironment (DesRochers et al., 2013; Wilmer et al., 2016).

Renal transporters are responsible for the reabsorption, secretion, and clearance of drugs and xenobiotics. Freshly isolated primary human renal proximal tubule cells (PTCs) are often used to assess renal physiology, but these cells are expensive and can dedifferentiate and lose expression of key transporters after cryopreservation (Zhang et al., 2015). Similarly, immortalized cells derived from the kidney retain only a subset of renal properties (Jenkinson et al., 2012; DesRochers et al., 2013; Tiong et al., 2014; Wilmer et al., 2016). As a result, these cell types show only minimal toxicity and small changes in renal injury biomarkers, such as kidney injury molecule 1 (KIM-1) and neutrophil gelatinase-associated lipocalin (NGAL), when exposed to known, in vivo nephrotoxic compounds (Huang et al., 2015). Therefore, a need exists for the development of more physiologically relevant models that better mimic in vivo kidney biology and can be used for nephrotoxicity studies.

Human pluripotent stem cells (hPSCs) are an attractive source for generating physiologically relevant in vitro models because of their inherent ability to differentiate into cells of the three germ layers. Studies have shown that hPSCs can be differentiated into three-dimensional

This work was supported by Pfizer's postdoctoral research program and at the time of data generation, all authors were compensated employees of Pfizer Inc.
https://doi.org/10.1124/dmd.118.082727.
[S]This article has supplemental material available at dmd.aspetjournals.org.

ABBREVIATIONS: ABC, ATP-binding cassette; APAP, acetaminophen; BCRP, breast cancer resistance protein; BSA, bovine serum albumin; CHIR99021, 6-[2-[[4-(2,4-dichlorophenyl)-5-(5-methyl-1*H*-imidazol-2-yl)pyrimidin-2-yl]amino]ethylamino]pyridine-3-carbonitrile; DMSO, dimethylsulfoxide; ECAD, E-cadherin; EG, ethylene glycol; FGF9, fibroblast growth factor 9; GGT, gamma glutamyltransferase; HO-1, heme oxygenase 1; hPSC, human pluripotent stem cells; KIM-1, kidney injury molecule 1; LTL, lotus tetragonolobus lectin; MATE, multidrug and toxin extrusion protein; MRP, multidrug resistance-associated protein; NPHS1, nephrin; OAT, organic anion transporter; OATP4C1, organic anion transporter polypeptide 4C1; OCT, organic cation transporter; OCTN2, organic cation transporter, novel, type 2; PBS, phosphate-buffered saline; PCR, polymerase chain reaction; PODXL, podocalyxin; PTC, proximal tubule cell; qRT-PCR, quantitative reverse-transcription polymerase chain reaction; SLC, solute carrier; 3D, three-dimensional; WT1, Wilms tumor protein; Y27632, 4-[(1*R*)-1-aminoethyl]-*N*-pyridin-4-ylcyclohexane-1-carboxamide.

(3D) multicellular cultures that contain many of the cell types found in the kidney, and these cultures develop structures reminiscent of early kidney architecture (Takasato et al., 2014, 2015; Morizane et al., 2015; Taguchi and Nishinakamura, 2015). Proximal tubule like structures within the cultures demonstrate some features of mature tubules, such as dextran uptake and sensitivity to the nephrotoxin cisplatin as demonstrated by induction of apoptosis or increases in markers of kidney damage such as KIM-1 or phosphorylated histone, γH2AX staining (Morizane et al., 2015; Takasato et al., 2015). Although these studies were primarily focused on developing an efficient differentiation protocol, they suggested that hPSC-derived kidney cultures could serve as a potential model for evaluating potentially nephrotoxic compounds.

In this study, we adapted one of the previously published protocols (Morizane et al., 2015) to generate multicellular kidney cultures and evaluate the ability of the cellular model to discriminate known nephrotoxins from benign compounds. The differentiated cells showed the activities of functional proximal tubules such as megalin-dependent cubilin-mediated endocytosis of fluorescently labeled dextran and active gamma-glutamyl transpeptidase (GGT), as well as functional expression of several important drug transporters. However, key renal transporters such as organic anion transporter 1 (OAT1), OAT3, and organic cation transporter 2 (OCT2) were only present at low levels. Nonetheless, we were also able to distinguish tubular toxicants from glomerular toxicants and benign compounds by using the gene expression levels of markers of renal damage KIM-1, heme oxygenase 1 (HO-1), and the ratio of the expression of nephrin (NPHS1) to Wilms tumor protein (WT1), two commonly expressed podocyte markers. These studies confirm the potential for hPSC-derived multicellular kidney cultures to serve as a model for evaluating potentially nephrotoxic compounds, assuming additional improvements can be made in the expression of key renal transporters.

Materials and Methods

Culture, Maintenance, and Differentiation of Cells. Undifferentiated H9 human embryonic stem cells were licensed from the Wisconsin Alumni Research Foundation. These cells were maintained in human embryonic stem cell medium and cultured on mouse embryonic fibroblasts on a P-100 tissue culture dish in a 37°C incubator with 6% CO_2. The cells were passaged using 1 mg/ml Dispase (cat. no. 17105-041; ThermoFisher Scientific, Waltham, MA) at 1:6 split ratio every 5–7 days. After every two to three passages, the cells were authenticated by testing for pluripotency markers and tested for mycoplasma infection.

Differentiation was always performed on feeder-free H9 cells. The cells were first transferred to a feeder-free culture system, which required culturing them on human embryonic stem cell–qualified Matrigel-coated (cat. no. 354277; BD Biosciences, San Jose, CA) P-100 dishes for at least two passages in mTeSR1 (cat. no. 05850; Stemcell Technologies, Vancouver, BC, Canada). The cells were passaged using Accutase (cat. no. A11105-01; ThermoFisher Scientific) cell dissociation reagent. After every split (approximately every 4–6 days), 200,000 cells were seeded onto Matrigel-coated P-100 plates in mTeSR1 supplemented with 2 μM Thiazovivin (cat. no. 3845; Tocris Bioscience, Bristol, United Kingdom) for 24 hours. Subsequent medium changes consisted of mTeSR1 medium without Thiazovivin supplementation.

Cell differentiation was achieved by adapting a previously published protocol (Morizane et al., 2015). Briefly, 20,000 cells/cm^2 were seeded onto 24-well plates coated with Matrigel in mTeSR1 supplemented with 10 μM Y27632 (4-[(1*R*)-1-aminoethyl]-*N*-pyridin-4-ylcyclohexane-1-carboxamide, cat. no. 1254; Tocris Bioscience). After 72 hours in mTeSR1, the cells were switched to differentiation media consisting of basal medium (Advanced RPMI-1640, cat. no. 12633-020; ThermoFisher Scientific) supplemented with 2 mM of GlutaMax (cat. no. 35050-061; ThermoFisher Scientific) supplemented with 8 μM CHIR99021 (6-[2-[[4-(2,4-dichlorophenyl)-5-(5-methyl-1*H*-imidazol-2-yl)pyrimidin-2-yl]amino]ethylamino] pyridine-3-carbonitrile, cat. no. 4423; Tocris Bioscience) and cultured for 96 hours to induce differentiation toward the late primitive streak.

To induce differentiation toward the late intermediate mesoderm, the differentiation medium was switched to basal medium supplemented with 10 ng/ml Activin A (cat. no. 338-AC-10/CF; R&D Systems, Minneapolis, MN), and the cells were cultured for 72 hours. Metanephric mesenchyme induction was achieved by culturing the late intermediate mesoderm cells in basal medium supplemented with 10 ng/ml fibroblast growth factor 9 (FGF9, cat. no. 273-F9-025/CF; R&D Systems) for 48 hours. After this, the cells were cultured in basal medium supplemented with 10 ng/ml FGF9 + 3 μM CHIR99021 for an additional 48 hours to differentiate cells them toward pretubular aggregates. To generate renal vesicles, the medium was changed to basal medium supplemented with 10 ng/ml FGF9 for an additional 72 hours.

Finally, the cells were cultured in the basal differentiation medium for 7–14 days without addition of any supplements to generate terminally differentiated kidney cells, which were used for characterization of renal transporters and nephrotoxins. During the entire 21–28 days of differentiation, the medium was replaced every other day. Figure 1A summarizes the entire differentiation procedure.

Quantitative Reverse-Transcription Polymerase Chain Reaction. RNA isolation and purification from cells were performed at specific time points using the RNeasy Mini Kit (74104; Qiagen, Valencia, CA), either manually or using the automated QIAcube. Tissue homogenization was achieved using QIAshredder (cat. no. 79654; Qiagen). The RNase-free DNase set was used for genomic DNA removal (cat. no. 79254; Qiagen). Total purified RNA or cell lysates before RNA isolation were stored at −80°C. The cDNA was synthesized from ≤2000 ng of RNA using the High-Capacity RNA-to-cDNA kit (cat. no. 4387406; ThermoFisher Scientific). Quantitative reverse-transcription polymerase chain reaction (qRT-PCR) was performed with TaqMan Fast Advanced Master Mix (cat. no. 4444557; ThermoFisher Scientific) using the ViiA 7 Real-Time PCR System (ThermoFisher Scientific).

All samples were run with two technical replicates. Data were normalized using housekeeping genes (Supplemental Table 1 lists all the TaqMan primers that were used in this study) and then normalized to control samples using $\Delta\Delta C_T$ method. The data are presented in the figures as fold expression ($2^{-\Delta\Delta C_T}$). The range of the fold change was generated by incorporating the S.D. within the fold difference, where minimum ($2^{-(\Delta\Delta C_T + SD)}$) and maximum ($2^{-(\Delta\Delta C_T - SD)}$) were defined accordingly.

Immunocytochemistry. The cells were fixed in 4% paraformaldehyde solution (cat. no. RT 15710; Electron Microscopy Sciences, Hatfield, PA) for 20 minutes at room temperature followed by three washes with phosphate-buffered saline (PBS). The fixed cells were permeabilized in 0.4% Triton X-100 (cat. no. T8787; Sigma-Aldrich, St. Louis, MO) for 15 minutes at room temperature followed by two washes with PBS.

The permeabilized cells were blocked with 10% bovine serum albumin (BSA) (cat. no. 15260037; ThermoFisher Scientific) at room temperature and were incubated with primary antibodies overnight at 4°C in 1% BSA. After three washes with PBS, the permeabilization step was repeated, and the cells were incubated with secondary antibodies in 1% BSA with Hoechst 33342 and 1 drop/ml Image-iT FX signal enhancer (cat. no. I36933; ThermoFisher Scientific) for 2 hours at 37°C in the dark.

The following antibodies and dilutions were used: fluorescein-labeled lotus tetragonolobus lectin (LTL) (1:200, cat. no. FL-1321; Vector Laboratories, Burlingame, CA), goat anti-E-cadherin (ECAD) (1:40, cat. no. AF648; R&D Systems), goat anti-podocalyxin (PODXL) (1:100, cat. no. AF1658; R&D systems), sheep anti-NPHS1 (1:60, cat. no. AF4269; R&D Systems). The cells were washed 3 times in PBS and were imaged using a fluorescent confocal microscope.

Functional Analysis of the Renal Cells. For the Dextran uptake studies, the cells on day 21 of differentiation were incubated with 10 μg/ml Alexa Fluor 555 Dextran (cat. no. D34679; ThermoFisher Scientific) for 24 hours. The cells were fixed and stained by LTL without permeabilization and then imaged. GGT activity in the cells was analyzed using the GGT assay kit (cat. no. MAK089; Sigma-Aldrich) following manufacturer's protocol. Briefly, cells were scratched off the wells from six-well plates using a pipette tip in 200 μl ice-cold GGT assay buffer. The cells were collected and added to 15-ml glass centrifuge tubes and kept on ice at 4°C. The cells were lysed and homogenized using a handheld sonicator. Bursts of sonication were given to the cell lysate in the tubes for about 15 seconds (6 times) while the tube was kept on ice. After all the tubes were sonicated, they were centrifuged at 13,000*g* for 10 minutes in a centrifuge cooled to 4°C to remove insoluble material. Supernatants were collected and evaluated according to the manufacturer's protocol. The GGT enzyme provided in the kit was used as the positive control, and fibroblasts, which show minimal GGT activity in vitro, were used as the negative control.

Radioactive Uptake Studies. Transport buffer was prepared at pH 7.4 using Hank's balanced salt solution supplemented with 20 mM HEPES, and 5.55 mM dextrose. Stock solutions of all compounds were made in 100% dimethylsulfoxide (DMSO, cat. no. D8418; Sigma-Aldrich), and all experiments were performed at a substrate concentration that was below the reported K_m (1% final DMSO in the assay). Specifically, ^{14}C-L-carnitine (1 μM, NEC797; PerkinElmer Life and

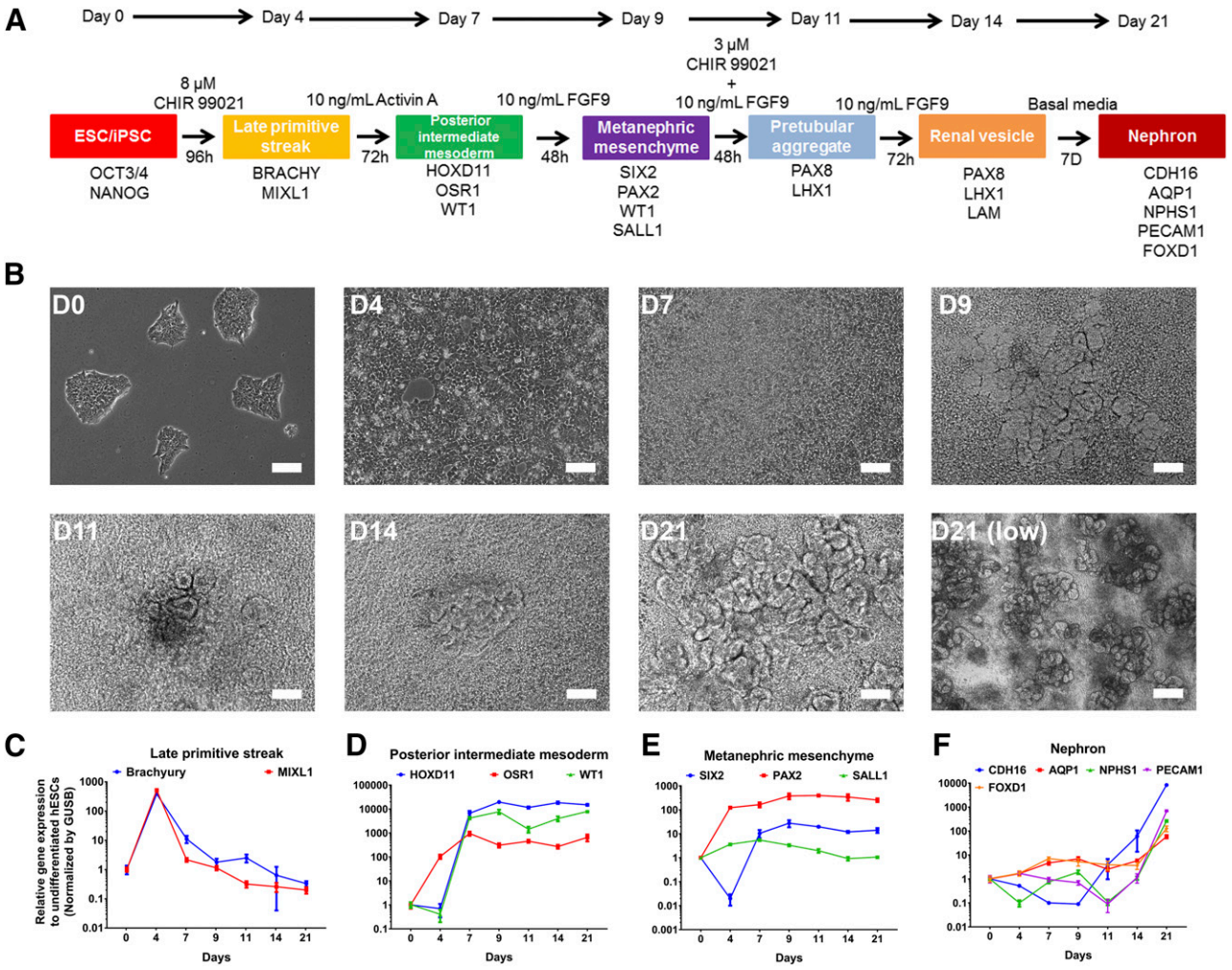

Fig. 1. Differentiation and characterization of H9 hPSCs to 3D multicellular structures containing renal cells. (A) Flow diagram highlighting the six-step protocol used for differentiating H9 embryonic stem cells to kidney cells. (B) Phase contrast images of the cells at each of the key steps involved during differentiation from pluripotent stem cells to fully differentiated kidney cells. Scale bars represent 100 μm except for D21-low where it represents 250 μm. (C–F) Time-course qRT-PCR for the key genes involved during differentiation of H9 cells to terminally differentiated kidney-like cells. Each data point was generated using at least three independent experiments. Data are presented as mean ± S.D.

Analytical Sciences, Waltham, MA), ^{3}H-digoxin (0.1 μM, NET222; PerkinElmer), and ^{14}C-metformin (10 μM, MC2043; Moravek Biochemicals and Radiochemicals, Brea, CA) were used as substrates for organic cation transporter, novel, type 2 (OCTN2), organic anion transporter polypeptide 4C1 (OATP4C1), and OCTs/multidrug and toxin extrusion proteins (MATEs), respectively. Cediranib (50 μM), ouabain (10 μM), and cimetidine (7 μM) (Pfizer Chemical Inventory System, Groton, CT) served as inhibitors of OCTN2, OATP4C1, and OCTs/-MATEs at the chosen final concentrations. Immediately before the experiment, cells on day 21 of differentiation were washed 3 times with 0.5 ml of transport buffer at room temperature and incubated with 0.5 ml of transport buffer with radiolabeled substrates (with and without inhibitors) at 37°C.

At the end of incubation (2, 5, 10, and 20 minutes), the cellular uptake was terminated by washing the cells 3 times with ice-cold transport buffer and lysing them with 0.4 ml of 1% sodium dodecyl sulfate in Dulbecco's PBS. The cells were subjected to shaking for 60 minutes. The accumulated radioactivity was determined by mixing the cell lysate with 4.0 ml of scintillation fluid (Bio-Safe II Complete Counting Cocktail, cat. no. 111196; Research Products International, Mount Prospect, IL). The radioactivity in each sample was quantified by measurement on a Wallac 1409 DSA Liquid Scintillation Counter (PerkinElmer).

Nephrotoxicity Assays. All compounds except gentamicin (cat. no. G1264; Sigma-Aldrich) and doxorubicin (cat. no. D1515; Sigma-Aldrich) were obtained from Pfizer Global Material Management (Groton, CT). All compounds except for gentamicin, doxorubicin, and puromycin were dissolved in DMSO, which was then dissolved in basal media. Cisplatin was dissolved in 0.5% dimethylformamide. The day-21 differentiated cells were incubated with either vehicle controls (0.5% DMSO or basal medium) or various concentrations of compounds (300 μM highest concentration).

After 24 hours of incubation, the cells were lysed with the RLT buffer, and gene expression analysis was performed. Tubular nephrotoxicity was assessed as a significant increase in KIM-1 or HO-1 gene expression as compared with baseline expression in vehicle control samples. Glomerular nephrotoxicity was assessed as a significant increase in the ratio of NPHS1 expression divided by WT1 expression as compared with the baseline ratio in vehicle control samples. Three independent experiments were performed for each compound at each dose, and the data presented are representative of the three experiments.

Statistical Analysis. Data analysis was performed using either MATLAB (MathWorks, Natick, MA) or Microsoft Excel (Redmond, WA) and graphs were generated using GraphPad Prism 6 (GraphPad Software, San Diego, CA). Data are presented as the mean ± S.D. unless otherwise stated. Comparison between two groups was performed using Student's *t* test or two-way analysis of variance (corrected for multiple comparisons), and $P < 0.05$ was considered statistically significant.

Results

Differentiation of H9 Cells Generates Multicellular Structures Expressing Markers of Kidney Cells. The mammalian kidney is derived from the cells of the intermediate mesoderm, which differentiates toward the metanephric mesenchyme, a nephron progenitor stage, and eventually gives rise to PTCs and podocytes (Little and McMahon,

2012). The protocol for differentiating H9 cells to different types of kidney cells is summarized in Fig. 1A. Treatment of the cells with CHIR99021, a glycogen synthase kinase 3β inhibitor that functions as a WNT activator, starting from the first day of differentiation led to rapid proliferation of cells and the initiation of a monolayer by day 4 (Fig. 1B). Treatment with activin A induced a confluent monolayer by day 7. The cells started to aggregate into small 3D structures by day 9 and increased in size with continued culture.

By day 21, a heterogeneous mix of PTCs, podocytes, and other renal cell types was observed (Fig. 1B), as determined by immunostaining and corroborated by gene expression analysis (Fig. 1, C–F). Brachyury and MIXL1, primitive streak markers, showed high levels of expression at the end of the first stage of differentiation (day 4) before decreasing to basal levels by later stages of differentiation (Fig. 1C).

The posterior intermediate mesoderm markers (HOXD11, WT1, and OSR1) sharply rose by day 7 (Fig. 1D) and then maintained these high levels for the remainder of the differentiation period. Metanephric mesenchyme markers peaked by day 9.

Markers of late-stage kidney differentiation—CDH16 (PTC marker), AQP1 (PTC marker), NPHS1 (podocyte marker), and PECAM1 (endothelial marker)—showed very low expression in the early differentiation process but increased sharply by day 21, suggesting commitment by the cells to a kidney fate (Fig. 1F). Additionally, strong expression of FOXD1 at the later stages of differentiation indicated the presence of renal stroma cells.

Collectively, the expression data confirmed that the differentiation protocol yielded multicellular structures consistent with kidney cell fates and structures reminiscent of early nephrogenesis.

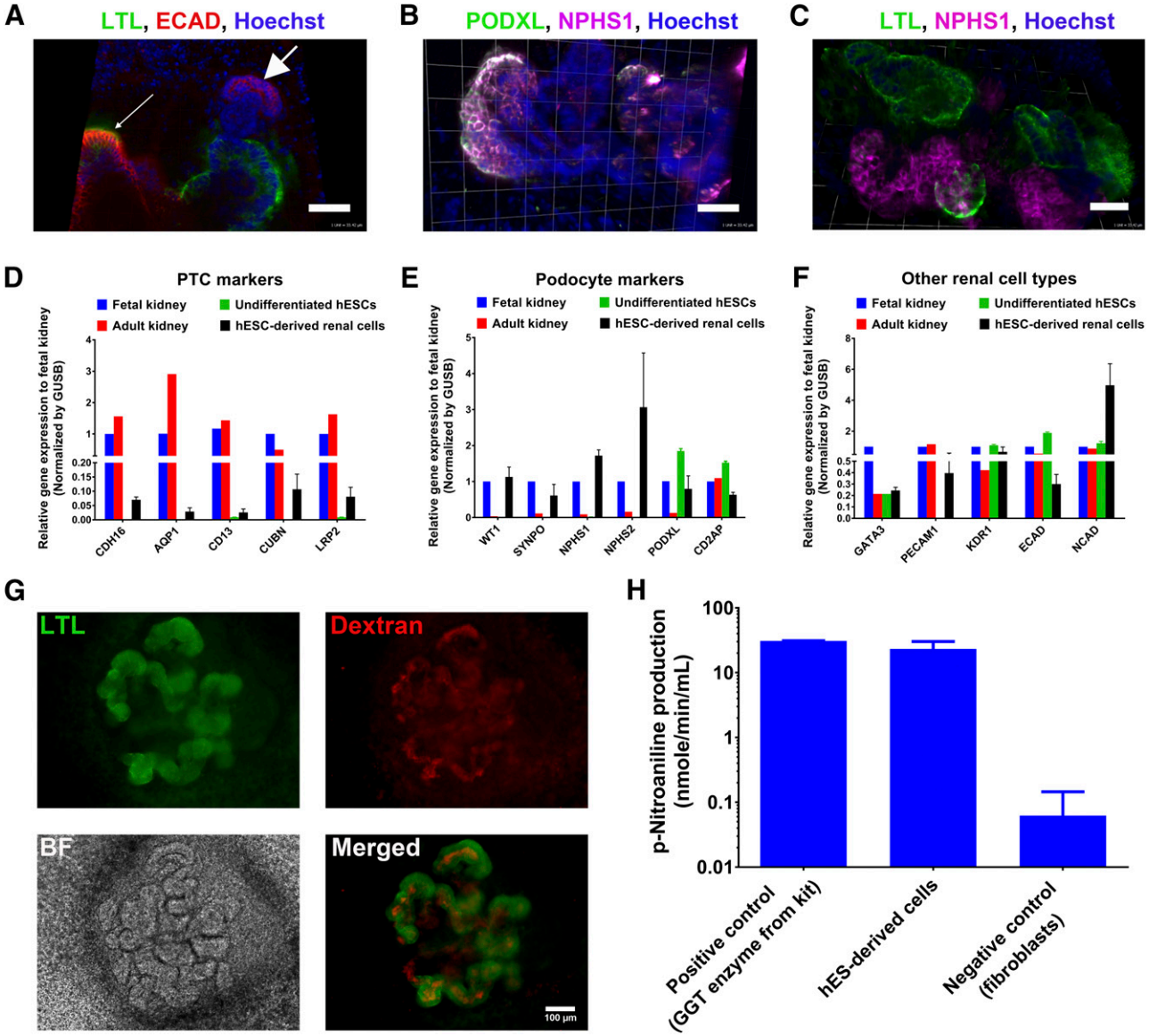

Fig. 2. Functional characterization of the 3D multicellular kidney structures. (A–C) Immunofluorescent images showing the presence of PTCs. (A) The thin arrow represents LTL^+ECAD^+ tubules, and thick arrow shows LTL^-ECAD^+ tubules, (B) podocytes ($NPHS1^+$ and $PODXL^+$), (C) podocytes ($NPHS1^+$) and PTCs (LTL^+). Scale bar, 50 μm. (D–F) Quantitative PCR for specific markers related to (D) PTCs, (E) podocytes, and (F) other cell types of the kidney. Gene expression for each of these specific markers is compared with fetal kidney tissue. Each data point was generated using two replicates from three independent experiments (n = 3). Data are presented as mean ± S.D. (G) Images (fluorescent and phase contrast) showing megalin-dependent cubilin-mediated endocytosis of fluorescently-labeled dextran. Scale bar: 100 μm. (H) Activity of gamma-glutamyl transpeptidase enzyme in the differentiated cells (n = 3). Data are presented as mean ± S.D.

3D Multicellular Kidney Structures Express Functional Renal Proteins. Immunostaining was used to identify specific cell types within the 3D multicellular structures after 21 days of differentiation. Expression of LTL^+ECAD^+ and LTL^-ECAD^+ 3D structures indicated the presence of PTCs and distal tubule-like structures, respectively (Fig. 2A) (Takasato et al., 2015). Glomerular podocytes as defined by $NPHS1^+PODXL^+$ cells can be seen in Fig. 2B. Podocytes comprising the Bowman's capsule as defined by $NPHS1^+$ cells can be seen adjacent to LTL^+ proximal tubule (Fig. 2C), suggesting that structures similar to the early segments of the nephron were generated using this protocol.

Gene expression studies confirmed the generation of specific kidney cell types after 21 days of differentiation. PTC-specific gene expression (CDH16, AQP1, aminopeptidase N [CD13], CUBN, LRP2) was significantly up-regulated compared with undifferentiated H9 cells, although significantly lower than expression in human fetal or adult kidney tissue (Fig. 2D). Podocyte-specific markers (WTI, SYNPO, NPHS1, NPHS2, PODXL, CD2AP) (Sharmin et al., 2016) were highly expressed (Fig. 2E). The epithelial markers ECAD and N-cadherin (NCAD) and markers for other renal cell types such as collecting duct (GATA3) and developing renal vasculature (KDR1, PECAM1) were also expressed (Fig. 2F).

To determine the functional activity of the multicellular structures, two assays were performed. The LTL^+ multicellular structures exhibited megalin-dependent cubilin-mediated uptake of fluorescent dextran (Fig. 2G). Megalin and cubilin are key endocytic receptors highly expressed in PTCs in the kidney and are responsible for the clearance of majority of the proteins filtered in the glomeruli (Christensen and Nielsen, 2007). The multicellular cultures also showed GGT activity (Fig. 2H). GGT, an enzyme uniquely located on the brush border of

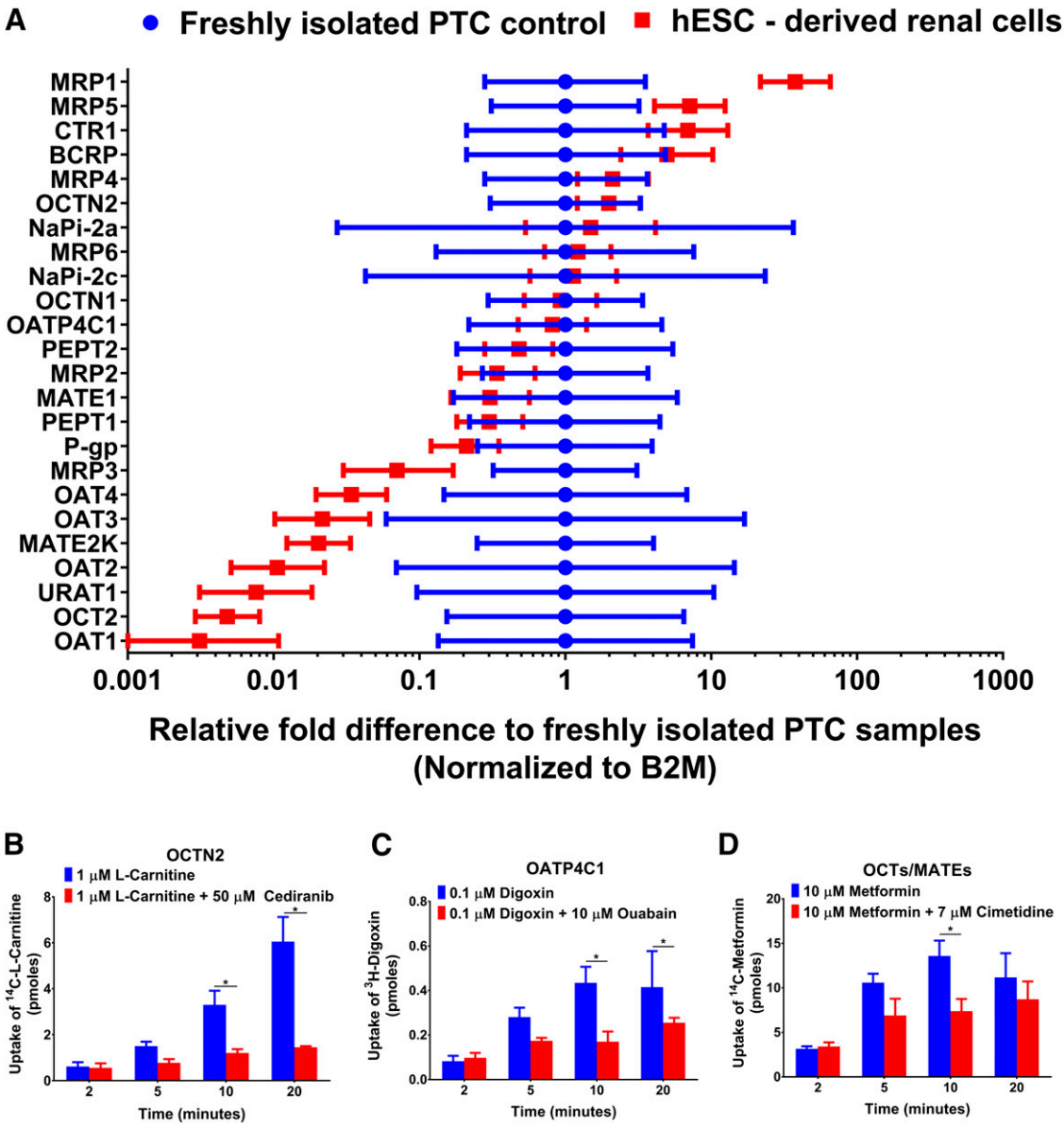

Fig. 3. Characterization of renal-specific transporters in the differentiated PTCs. (A) Quantitative PCR showing the expression levels of 24-renal specific transporters from both the ABC and SLC family relative to freshly isolated PTCs from three donors. Each data point was generated from at least three independent experiments. Data are presented as mean ± minimum/maximum ($n = 3$). (B–D) Uptake studies with and without inhibitors for three different transporters: (B) OCTN2, (C) OATP4C1, and (D) OCTs/MATEs. Data are presented as mean ± S.D. ($n = 3$). Statistical significance was determined using two-way analysis of variance, and $^*P < 0.05$ is considered statistically significant.

PTCs, has also been used as a diagnostic marker for renal ischemic injury (Ward, 1975).

Taken together, these results indicate that a heterogenous mixture of kidney cell types developed in the multicellular structures. Although these structures resemble early nephrons and have functional activity associated with kidney cells, they do not perfectly match the cellular composition or maturity of adult nephrons.

3D Multicellular Kidney Structures Express Functional Renal Transporters. Renal cells are involved in the elimination of drugs, xenobiotics, and toxins, a task that is accomplished by apical and basolateral transporters (Inui et al., 2000). These transporters are essential for the movement of organic anions and cations where elimination by urine, enabled by transport through the PTCs, is a major pathway in the detoxification process. RNA from freshly isolated PTCs from three individual adult donors (Supplemental Table 2) was used as a control to compare the transporter expression with 21-day differentiated hPSC-derived kidney cells.

Of the 24 PTC transporters investigated, 16 were expressed at or above the levels of the control PTC samples (Fig. 3A), which is better than reported in other non-hPSC reported kidney models (Jenkinson et al., 2012; Zhang et al., 2015). Transporters expressed at physiological levels included the major efflux transporters located on the apical side of the PTCs: multidrug resistance-associated protein 2 (ABCC2, also known as MRP2), ABCC4 (MRP4), and P-glycoprotein (Smeets et al., 2004); transporters responsible for the absorption of small peptides: solute carrier 15A1 (SLC15A1, also known as peptide transporter 1 (PEPT1) and SLC15A2 (peptide transporter2, PEPT2) (Daniel and Rubio-Aliaga, 2003); transporters that mediate the reabsorption of inorganic phosphate: SLC34A1 (NaPi-2a) and SLC34A3 (NaPi-2c) (Biber et al., 2013); and transporters responsible for the absorption of ergothioneine and L-carnitine: SLC22A4 (OCTN1), SLC22A5 (OCTN2) (Gründemann, 2012). Additionally, expression of SLCO4C1 (OATP4C1), the basolateral transporter involved in the uptake of digoxin, was also observed in the differentiated cells (Mikkaichi et al., 2004). Gene expression of OAT1, OAT3, and OCT2 was observed at low levels compared with the PTC controls, suggesting that although the differentiated cells demonstrated many transporters associated with in vivo PTCs, additional protocol optimization or maturation is still required to capture the entire complexity of kidney transporter gene expression.

To determine whether a subset of the expressed transporters were functional, we monitored the transporter mediated uptake of radiolabeled substrates on day 21 of differentiation. L-carnitine (OCTN2), digoxin (OATP4C1), and metformin (OCTs/MATEs) were evaluated using reported K_m values (Mikkaichi et al., 2004; Morrissey et al., 2012; Johnston et al., 2014; Drug Interaction Database 2018). As shown in Fig. 3, B–D, time-dependent cellular uptake was evident for all three substrates. As expected, the substrate transport was inhibited with known inhibitors for OCTN2 (50 μM cediranib, maximum inhibition of 76% at 20 minutes), OATP4C1 (10 μM ouabain, maximum inhibition of 60% at 10 minutes), and OCTs/MATEs (7 μM cimetidine, maximum inhibition of 46% at 10 minutes).

As metformin is a substrate for OCT2, MATE1, and MATE2K (Morrissey et al., 2013), we cannot conclusively determine which of these transporters was responsible for its uptake. Additional studies are needed to tease out the transporter(s) involved in the uptake of metformin as MATEs can be involved in both uptake and efflux of compounds depending on the proton gradient (Yonezawa and Inui, 2011).

3D Multicellular Kidney Cultures can Distinguish between Glomerular Toxicants, Tubular Toxicants, and Benign Compounds by Monitoring Key Renal Markers. To determine whether the 3D multicellular kidney cultures can be used to distinguish between nephrotoxins and benign compounds, six kidney tubular toxins, two glomerular toxins, and two benign compounds were selected for a proof-of-concept study. Expression of four genes were monitored as indicators of cellular damage. Two markers were monitored, KIM-1 and HO-1, which have been demonstrated to increase after kidney tubular injury (Han et al., 2002; Adler et al., 2016). Additionally, because most current kidney biomarkers such as cystatin C, α1-microglobulin, and β2-macroglobulin (Vaidya et al., 2008) cannot differentiate between glomerular and tubular injury, we used a ratio of two commonly expressed podocyte-specific expressed genes, NPHS1 and WT1, as a marker for glomerular damage. Cells were treated for 24 hours with increasing concentrations of compounds followed by gene expression analysis.

The model was able to correctly identify four tubular toxicants (gentamicin, citrinin, cisplatin, and rifampicin) as evidenced by an increase in the tubular biomarkers KIM-1 and HO-1 (Fig. 4A). Interestingly, HO-1 levels were always higher that KIM-1, suggesting that in this system HO-1 was the more sensitive injury biomarker. Similar observations have been reported previously by Adler et al. (2016), who showed a robust increase in HO-1 levels compared with only a modest increase in KIM-1 levels after subjecting primary tubular cells to $CdCl_2$, a potent tubular toxicant. Neither acetaminophen (APAP) or ethylene glycol (EG), which are also tubular toxicants in vivo, showed an increase in markers of renal cellular damage.

When the differentiated cells were subjected to doxorubicin and puromycin, primarily glomerular toxicants, increased levels of NPHS1/WT1 was observed (Fig. 4B). There was no increase in the ratio of NPHS1/WT1 when these cells were subjected to primarily tubular toxins (Fig. 4A), suggesting that the in vitro model is also able to distinguish glomerular injury from tubular injury.

Finally, when the cells were treated with benign compounds (acarbose and ribavirin), no statistically significant increase was observed for any of the three markers (Fig. 4C). These results indicate that the 3D multicellular kidney cultures were able to classify the compounds as tubular toxins, glomerular toxins, or benign compounds.

Discussion

In this study, we differentiated hPSCs to 3D multicellular structures containing a variety of renal cells by recapitulating elements of in vivo nephrogenesis as evidenced by sequential expression of markers of renal progenitors and terminally differentiated cells. The differentiated cells were characterized by gene expression analysis, immunostaining, and functional studies.

The cells exhibited dextran uptake by megalin-dependent and cubilin-mediated receptors and GGT enzyme activity, suggesting that functional PTCs were present. However, gene expression data also indicated much lower expression of PTC-specific genes compared with both adult and fetal kidneys. In contrast, podocyte markers were expressed at levels comparable or higher than adult and fetal kidneys. These data indicate that there is a heterogenous mixture of different cell types in the differentiated cells, all of which are not fully mature. This is likely due at least in part to the unorganized differentiation of the cells that generate 3D multicellular structures of various cellular compositions. Additional protocol optimization and maturation is likely required to generate a model that more faithfully replicates normal kidney development and structure.

Despite the limitations of the differentiation protocol, the multicellular structures expressed more renal transporters than many routinely used, non-hPSC-derived kidney models (Jenkinson et al., 2012; Zhang et al., 2015). One transporter that was surprisingly well expressed was breast cancer resistance protein (BCRP). There are conflicting reports in the

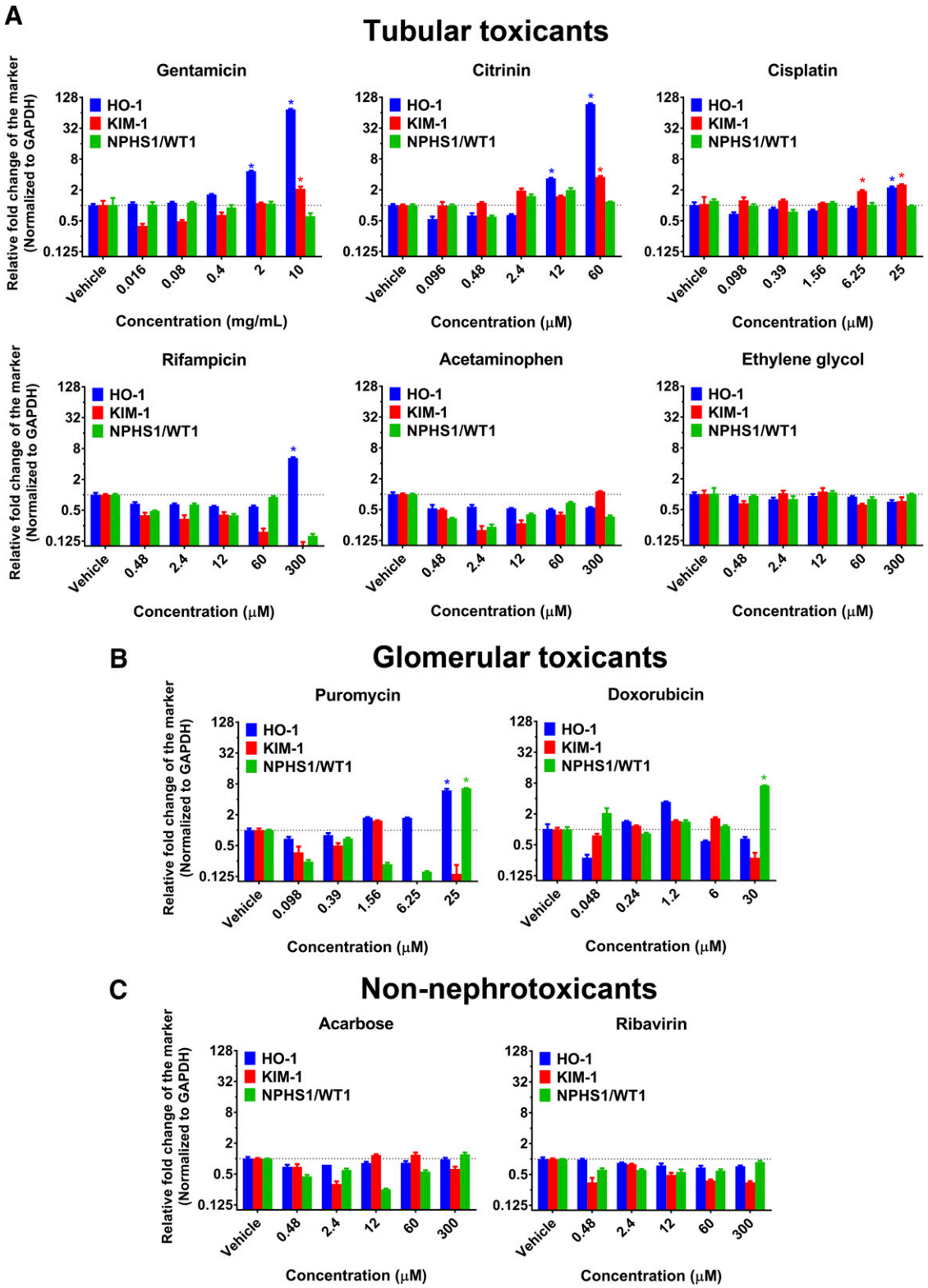

Fig. 4. Toxicity testing using differentiated kidney cells. Application of (A) tubular toxicants, (B) glomerular toxicants, and (C) non-nephrotoxicants to the in vitro kidney model. The experiment was performed three independent times, and the data presented here are representative of one of the three runs. Data are presented as mean ± S.D. Dashed lines on the graphs show the level of vehicle control. Statistical significance was tested for each of the three independent runs and was determined using Student's *t* test; $*P < 0.05$ is considered statistically significant.

literature regarding the presence of BCRP in human kidney PTCs. Huls et al. (2008) demonstrated the presence of BCRP mRNA in the human kidney and localized BCRP to the brush border of the proximal tubule cells by immunostaining. These researchers also showed that BCRP expression was comparable to other ATP-binding cassette (ABC) transporters such as P-glycoprotein, MRP2, and MRP4 in humans. In

contrast, Prasad et al. (2016) used targeted proteomics to detect BCRP protein in the kidney cortex, but argued its levels were below the limit of quantitation. In our stem cell–derived model, BCRP expression was comparable to MRP4 expression, supporting the observations made by Huls et al. (2008).

Having demonstrated that the 3D multicellular structures possessed many features representative of PTCs and podocytes, the primary purpose of our work was to evaluate the potential of the model to detect nephrotoxins. Six presentative tubular toxins were evaluated. Gentamicin uptake in PTCs is mediated by endocytosis, mediated by megalin and cubilin (Quiros et al., 2011). Citrinin, a food-derived mycotoxin, requires OAT1-mediated uptake for accumulation inside the PTCs (Kandasamy et al., 2015). Both rifampicin and cisplatin are substrates for OCT2 transporter (Yokoo et al., 2007; Kandasamy et al., 2015). Both puromycin and doxorubicin lead to glomerular damage and proteinuria (Jeansson et al., 2009). APAP toxicity requires biotransformation (Mazer and Perrone, 2008), and EG leads to toxicity via formation of oxalate crystals (Hovda et al., 2010). Acarbose and ribavirin are generally considered to be benign (Li et al., 2013, 2014; Kandasamy et al., 2015).

Gentamicin showed a sharp increase in HO-1 mRNA levels at concentrations $\geq$2 mg/ml. This matches well with previously published reports where gentamicin toxicity was observed at 1 to 2 mg/ml (Quiros et al., 2011). Citrinin produces tubular necrosis by its accumulation inside the PTCs (Berndt, 1998), and robust changes in both HO-1 and KIM-1 levels were seen after citrinin treatment at concentrations comparable to previous studies in primary PTCs (Adler et al., 2016).

Cisplatin, one of the most potent and widely used chemotherapy drugs, demonstrated a statistically significant increase in KIM-1 and HO-1 at concentrations lower than those used in primary a PTC model (Jang et al., 2013) and other hPSC-derived models (Morizane et al., 2015; Takasato et al., 2015). As rifampicin uptake is primarily mediated by OCT2, which is expressed at lower levels in this model, changes in HO-1 were only seen at the highest dose and KIM-1 did not show any significant difference in expression for this compound, suggesting that HO-1 was a more sensitive injury marker than KIM-1 in some instances.

It is noteworthy that the known tubular toxins gentamicin, citrinin, cisplatin, and rifampicin did not significantly change the ratio for NPHS1/WT1, up to the highest tested doses. Neither APAP or EG induced toxicity in our model, although, both these compounds are reported to be tubular nephrotoxins in vivo. For APAP, nephrotoxicity is associated with high doses, and cytochrome P450 2E1 (CYP2E1) metabolism is required for its biotransformation (Mazer and Perrone, 2008). However, Knights et al. (2013) indicated that CYP2E1 is not expressed in the human kidney.

Because we did not profile for any drug-metabolizing enzymes in the differentiated cells, we cannot conclusively determine the reason why our stem cell–derived model could not detect APAP nephrotoxicity. In the case of EG, it is initially metabolized by P450 enzymes in the liver, resulting in the formation of oxalic acid, which concentrates in the kidney and precipitates as calcium oxalate monohydrate crystals causing nephrotoxicity; this process would not be expected in an in vitro kidney model (El Menyiy et al., 2016). Our results are consistent with previous studies using primary PTCs that did not detect APAP or EG based nephrotoxicity either (Li et al., 2013, 2014; Adler et al., 2016).

Two glomerular/podocyte toxins were also evaluated. Puromycin, which is a primary glomerular toxicant and a secondary a tubular toxicant, exhibited statistically significant increased levels of both NPHS1/WT1 and HO-1, with the increase in NPHS1/WT1 being slightly more than the tubular marker. Doxorubicin treatment showed increased NPHS1/WT1 levels at 30 μM; this is consistent with studies showing that zebrafish embryos treated with 10–20 μM doxorubicin exhibited altered podocyte development with functional impairment and reduction of NPHS1 and WT1 (Zennaro et al., 2014). Although changes in NPHS1 and WT1 expression level are seen when subjected to glomerular toxicants, additional studies need to be done to confirm the sensitivity of these markers for toxicity. Previous studies have shown that acarbose and ribavirin do not cause kidney damage (Kandasamy et al., 2015), and our model confirmed these findings, suggesting that the model is suitable for distinguishing nephrotoxic compounds from benign compounds.

Among the various cell types of the kidney, tubular cells and glomerular podocytes are most prone to a toxic insult because of their location and function in the kidney. It has been extremely hard to classify this type of injury (tubular versus glomerular) because of the lack of specific markers for each type of injury and the difficulty of coculturing these PTCs and podocytes together in vitro. One benefit of the model we have presented here is the heterogeneous mixture of renal cells in the 3D multicellular structures. Using this model, we were able to identify the type of insult by evaluating the expression of well-accepted tubular injury markers (KIM-1, HO-1) compared with ratio of NPHS1/WT1. To our knowledge, this is the first model to distinguish between different types of kidney toxicity by monitoring changes in the expression levels of the cell-specific markers.

Although promising, this model requires further optimization, characterization, and validation. Key challenges of heterogeneity in stem cell differentiation and long-term expansion of cells need to be addressed. Recently, a report indicated that with appropriate 3D culture conditions it is possible to support the long-term culture of nephron progenitor cells from both primary fetal kidney as well as stem cells (Li et al., 2016). Furthermore, researchers from the University of Washington were able to perform a very similar hPSC-differentiation protocol to generate kidney organoids in a fully automated manner using liquid handing robots in both 96- and 384-well plates (Czerniecki et al., 2018). Such technologies as well as the ability to cryopreserve and efficiently thaw these cells without loss of key proteins can streamline the use of such models.

Various additional strategies could be applied to increase the expression of lowly expressed but important renal transporters. In an attempt to increase the expression levels of the more lowly expressed transporters, we extended the final differentiation phase (days 14–21) from 7 to 14 days (Supplemental Fig. 1) based on work that had shown that hPSC-derived cardiomyocytes acquired more adult-like gene expression patterns when cultured for 120 days (Babiarz et al., 2012). Not surprisingly, the overall gene expression pattern for the kidney transporters did not increase with the additional 7-day culture time, and we deemed the longer protocol intractable for routine use in nephrotoxicity testing.

Previous literature has shown that fluidic shear stress can lead to functional maturation of the cells (Jang et al., 2013; Weber et al., 2016). Primary human kidney PTCs showed improved OAT1 and OAT3 inhibition by probenecid in microfluidic chips compared with their static counterparts (Weber et al., 2016). Similar results were observed by Jang et al. (2013), who found that inhibition of OCT2 by cimetidine significantly decreased apoptosis of the PTCs by cisplatin-mediated injury. Recently, it was shown that modulation of Nedd4-2, as well as serum and glucocorticoid inducible kinases, could improve the expression of OAT1 and OAT3 (Xu et al., 2016a,b). Thus, application of microfluidic shear along with kinase modulation could potentially lead to further improvement of our in vitro model with respect to the transporters, but it was outside the scope of the present work.

Stem cell–derived in vitro models are an exciting area of research and many pharmaceutical companies are actively looking for human in vitro models that more closely match human in vivo physiology. Our work demonstrates that hPSC-derived, 3D multicellular kidney models can discriminate nephrotoxins from benign compounds. Although the model

requires improvements to make it competitive with currently used primary cell models and must be tested with a much wider range of compounds, it offers the possibility of harnessing the attractive features of stem cell–based models, such as lower cost, greater flexibility, and patient and genetic diversity.

Acknowledgments

We would like to thank William Blake, Regis Doyonnas, and Yvonne Will for helpful discussions.

Authorship Contributions

Participated in research design: Bajaj, Rodrigues, Steppan, Engle, Mathialagan, Schroeter.

Conducted experiments: Bajaj, Mathialagan.

Contributed new reagents or analytic tools: Bajaj.

Performed data analysis: Bajaj, Mathialagan.

Wrote or contributed to the writing of the manuscript: Bajaj, Rodrigues, Steppan, Engle, Mathialagan, Schroeter.

References

Adler M, Ramm S, Hafner M, Muhlich JL, Gottwald EM, Weber E, Jaklic A, Ajay AK, Svoboda D, Auerbach S, et al. (2016) A quantitative approach to screen for nephrotoxic compounds in vitro. *J Am Soc Nephrol* **27**:1015–1028.

Babiarz JE, Ravon M, Sridhar S, Ravindran P, Swanson B, Bitter H, Weiser T, Chiao E, Certa U, and Kolaja KL (2012) Determination of the human cardiomyocyte mRNA and miRNA differentiation network by fine-scale profiling. *Stem Cells Dev* **21**:1956–1965.

Berndt WO (1998) The role of transport in chemical nephrotoxicity. *Toxicol Pathol* **26**:52–57.

Biber J, Hernando N, and Forster I (2013) Phosphate transporters and their function. *Annu Rev Physiol* **75**:535–550.

Bonventre JV, Vaidya VS, Schmouder R, Feig P, and Dieterle F (2010) Next-generation biomarkers for detecting kidney toxicity. *Nat Biotechnol* **28**:436–440.

Christensen EI and Nielsen R (2007) Role of megalin and cubilin in renal physiology and pathophysiology. *Rev Physiol Biochem Pharmacol* **158**:1–22.

Czerniecki SM, Cruz NM, Harder JL, Menon R, Annis J, Otto EA, Gulieva RE, Islas LV, Kim YK, Tran LM, et al. (2018) High-throughput screening enhances kidney organoid differentiation from human pluripotent stem cells and enables automated multidimensional phenotyping. *Cell Stem Cell* **22**:929–940.e4.

Daniel H and Rubio-Aliaga I (2003) An update on renal peptide transporters. *Am J Physiol Renal Physiol* **284**:F885–F892.

DesRochers TM, Suter L, Roth A, and Kaplan DL (2013) Bioengineered 3D human kidney tissue, a platform for the determination of nephrotoxicity. *PLoS One* **8**:e59219.

El Menyiy N, Al Waili N, Bakour M, Al-Waili H, and Lyoussi B (2016) Protective effect of propolis in proteinuria, crystaluria, nephrotoxicity and hepatotoxicity induced by ethylene glycol ingestion. *Arch Med Res* **47**:526–534.

Gründemann D (2012) The ergothioneine transporter controls and indicates ergothioneine activity--a review. *Prev Med* **54** (Suppl):S71–S74.

Han WK, Bailly V, Abichandani R, Thadhani R, and Bonventre JV (2002) Kidney injury molecule-1 (KIM-1): a novel biomarker for human renal proximal tubule injury. *Kidney Int* **62**:237–244.

Hovda KE, Guo C, Austin R, and McMartin KE (2010) Renal toxicity of ethylene glycol results from internalization of calcium oxalate crystals by proximal tubule cells. *Toxicol Lett* **192**:365–372.

Huang JX, Kaeslin G, Ranall MV, Blaskovich MA, Becker B, Butler MS, Little MH, Lash LH, and Cooper MA (2015) Evaluation of biomarkers for in vitro prediction of drug-induced nephrotoxicity: comparison of HK-2, immortalized human proximal tubule epithelial, and primary cultures of human proximal tubular cells. *Pharmacol Res Perspect* **3**:e00148.

Huls M, Brown CDA, Windass AS, Sayer R, van den Heuvel JJMW, Heemskerk S, Russel FGM, and Masereeuw R (2008) The breast cancer resistance protein transporter ABCG2 is expressed in the human kidney proximal tubule apical membrane. *Kidney Int* **73**:220–225.

Inui KI, Masuda S, and Saito H (2000) Cellular and molecular aspects of drug transport in the kidney. *Kidney Int* **58**:944–958.

Jang KJ, Mehr AP, Hamilton GA, McPartlin LA, Chung S, Suh KY, and Ingber DE (2013) Human kidney proximal tubule-on-a-chip for drug transport and nephrotoxicity assessment. *Integr Biol* **5**:1119–1129.

Jeansson M, Björck K, Tenstad O, and Haraldsson B (2009) Adriamycin alters glomerular endothelium to induce proteinuria. *J Am Soc Nephrol* **20**:114–122.

Jenkinson SE, Chung GW, van Loon E, Bakar NS, Dalzell AM, and Brown CD (2012) The limitations of renal epithelial cell line HK-2 as a model of drug transporter expression and function in the proximal tubule. *Pflugers Arch* **464**:601–611.

Johnston RA, Rawling T, Chan T, Zhou F, and Murray M (2014) Selective inhibition of human solute carrier transporters by multikinase inhibitors. *Drug Metab Dispos* **42**:1851–1857.

Kandasamy K, Chuah JKC, Su R, Huang P, Eng KG, Xiong S, Li Y, Chia CS, Loo L-H, and Zink D (2015) Prediction of drug-induced nephrotoxicity and injury mechanisms with human induced pluripotent stem cell-derived cells and machine learning methods. *Sci Rep* **5**:12337.

Knights KM, Rowland A, and Miners JO (2013) Renal drug metabolism in humans: the potential for drug-endobiotic interactions involving cytochrome P450 (CYP) and UDP-glucuronosyltransferase (UGT). *Br J Clin Pharmacol* **76**:587–602.

Li Y, Kandasamy K, Chuah JK, Lam YN, Toh WS, Oo ZY, and Zink D (2014) Identification of nephrotoxic compounds with embryonic stem-cell-derived human renal proximal tubular-like cells. *Mol Pharm* **11**:1982–1990.

Li Y, Oo ZY, Chang SY, Huang P, Eng KG, Zeng JL, Kaestli AJ, Gopalan B, Kandasamy K, Tasnim F, et al. (2013) An in vitro method for the prediction of renal proximal tubular toxicity in humans. *Toxicol Res* **2**:352–365.

Li Z, Araoka T, Wu J, Liao H-K, Li M, Lazo M, Zhou B, Sui Y, Wu M-Z, Tamura I, et al. (2016) 3D culture supports long-term expansion of mouse and human nephrogenic progenitors. *Cell Stem Cell* **19**:516–529.

Little MH and McMahon AP (2012) Mammalian kidney development: principles, progress, and projections. *Cold Spring Harb Perspect Biol* **4**:a008300.

Mazer M and Perrone J (2008) Acetaminophen-induced nephrotoxicity: pathophysiology, clinical manifestations, and management. *J Med Toxicol* **4**:2–6.

Mikkaichi T, Suzuki T, Onogawa T, Tanemoto M, Mizutamari H, Okada M, Chaki T, Masuda S, Tokui T, Eto N, et al. (2004) Isolation and characterization of a digoxin transporter and its rat homologue expressed in the kidney. *Proc Natl Acad Sci USA* **101**:3569–3574.

Morizane R, Lam AQ, Freedman BS, Kishi S, Valerius MT, and Bonventre JV (2015) Nephron organoids derived from human pluripotent stem cells model kidney development and injury. *Nat Biotechnol* **33**:1193–1200.

Morrissey KM, Stocker SL, Wittwer MB, Xu L, and Giacomini KM (2013) Renal transporters in drug development. *Annu Rev Pharmacol Toxicol* **53**:503–529.

Morrissey KM, Wen CC, Johns SJ, Zhang L, Huang SM, and Giacomini KM (2012) The UCSF-FDA TransPortal: a public drug transporter database. *Clin Pharmacol Ther* **92**:545–546.

Prasad B, Johnson K, Billington S, Lee C, Chung GW, Brown CDA, Kelly EJ, Himmelfarb J, and Unadkat JD (2016) Abundance of drug transporters in the human kidney cortex as quantified by quantitative targeted proteomics. *Drug Metab Dispos* **44**:1920–1924.

Quiros Y, Vicente-Vicente L, Morales AI, López-Novoa JM, and López-Hernández FJ (2011) An integrative overview on the mechanisms underlying the renal tubular cytotoxicity of gentamicin. *Toxicol Sci* **119**:245–256.

Drug Interaction Database Program (2018), https://www.druginteractioninfo.org. Ragueneau-Majlessi I, contact. Department of Pharmaceutics, School of Pharmacy, University of Washington, Seattle, WA.

Sharmin S, Taguchi A, Kaku Y, Yoshimura Y, Ohmori T, Sakuma T, Mukoyama M, Yamamoto T, Kurihara H, and Nishinakamura R (2016) Human induced pluripotent stem cell-derived podocytes mature into vascularized glomeruli upon experimental transplantation. *J Am Soc Nephrol* **27**:1778–1791.

Smeets PH, van Aubel RA, Wouterse AC, van den Heuvel JJ, and Russel FG (2004) Contribution of multidrug resistance protein 2 (MRP2/ABCC2) to the renal excretion of p-aminohippurate (PAH) and identification of MRP4 (ABCC4) as a novel PAH transporter. *J Am Soc Nephrol* **15**:2828–2835.

Taguchi A and Nishinakamura R (2015) Nephron reconstitution from pluripotent stem cells. *Kidney Int* **87**:894–900.

Takasato M, Er PX, Becroft M, Vanslambrouck JM, Stanley EG, Elefanty AG, and Little MH (2014) Directing human embryonic stem cell differentiation towards a renal lineage generates a self-organizing kidney. *Nat Cell Biol* **16**:118–126.

Takasato M, Er PX, Chiu HS, Maier B, Baillie GJ, Ferguson C, Parton RG, Wolvetang EJ, Roost MS, Chuva de Sousa Lopes SM, et al. (2015) Kidney organoids from human iPS cells contain multiple lineages and model human nephrogenesis. *Nature* **526**:564–568.

Tiong HY, Huang P, Xiong S, Li Y, Vathsala A, and Zink D (2014) Drug-induced nephrotoxicity: clinical impact and preclinical in vitro models. *Mol Pharm* **11**:1933–1948.

Vaidya VS, Ferguson MA, and Bonventre JV (2008) Biomarkers of acute kidney injury. *Annu Rev Pharmacol Toxicol* **48**:463–493.

Ward JP (1975) Gamma-glutamyl transpeptidase. A sensitive indicator of renal ischaemic injury in experimental animals and renal homograft rejection in man. *Ann R Coll Surg Engl* **57**:248–261.

Weber EJ, Chapron A, Chapron BD, Voellinger JL, Lidberg KA, Yeung CK, Wang Z, Yamaura Y, Hailey DW, Neumann T, et al. (2016) Development of a microphysiological model of human kidney proximal tubule function. *Kidney Int* **90**:627–637.

Wilmer MJ, Ng CP, Lanz HL, Vulto P, Suter-Dick L, and Masereeuw R (2016) Kidney-on-a-chip technology for drug-induced nephrotoxicity screening. *Trends Biotechnol* **34**:156–170.

Xu D, Huang H, Toh MF, and You G (2016a) Serum- and glucocorticoid-inducible kinase sgk2 stimulates the transport activity of human organic anion transporters 1 by enhancing the stability of the transporter. *Int J Biochem Mol Biol* **7**:19–26.

Xu D, Wang H, and You G (2016b) An essential role of Nedd4-2 in the ubiquitination, expression, and function of organic anion Transporter-3. *Mol Pharm* **13**:621–630.

Yokoo S, Yonezawa A, Masuda S, Fukatsu A, Katsura T, and Inui K (2007) Differential contribution of organic cation transporters, OCT2 and MATE1, in platinum agent-induced nephrotoxicity. *Biochem Pharmacol* **74**:477–487.

Yonezawa A and Inui K (2011) Importance of the multidrug and toxin extrusion MATE/SLC47A family to pharmacokinetics, pharmacodynamics/toxicodynamics and pharmacogenomics. *Br J Pharmacol* **164**:1817–1825.

Zennaro C, Mariotti M, Carraro M, Pasqualetti S, Corbelli A, Armelloni S, Li M, Ikehata M, Clai M, Artero M, et al. (2014) Podocyte developmental defects caused by adriamycin in zebrafish embryos and larvae: a novel model of glomerular damage. *PLoS One* **9**:e98131.

Zhang X, Wang R, Piotrowski M, Zhang H, and Leach KL (2015) Intracellular concentrations determine the cytotoxicity of adefovir, cidofovir and tenofovir. *Toxicol In Vitro* **29**:251–258.

Address correspondence to: Dr. Thomas Schroeter, Discovery Sciences, Pfizer Worldwide Research and Development, Eastern Point Road, Groton, CT 06340. E-mail: Thomas.Schroeter@pfizer.com; or Dr. Piyush Bajaj, Global Investigative Toxicology, Drug Safety Research and Evaluation, 35 Landsdowne Street, Cambridge, MA 02139. E-mail: Piyush.Bajaj@takeda.com

Human Pluripotent Stem Cell Derived Kidney Model for Nephrotoxicity Studies

Piyush Bajaj, A. David Rodrigues, Claire M. Steppan, Sandra J. Engle, Sumathy Mathialagan, Thomas Schroeter

Drug Metabolism and Disposition manuscript # 82727

Legend for figures:

Supplementary Figure 1: qPCR showing the expression levels of 24 renal specific transporters from both the ABC- and SLC-family relative to freshly isolated PTCs from three-donors by extending the final maturation phase from 7 days to 14 days. (A) 9 days (B) 11 days (C) 14 days. Each data point was generated from at least three independent experiments. Data is presented as mean ± minimum/maximum *(n =3).*

Supplemental table 1: TaqMan primers and their assay ID used in the study.

Gene name	TaqMan assay ID
T (Brachury)	Hs00610080_m1
MIXL1	Hs04400364_m1
PAX2	Hs010574416_m1
LHX1	Hs00232144_m1
OSR1	Hs01586544_m1
SIX2	Hs00232731_m1
HOXD11	Hs00360798_m1
SALL1	Hs01548765_m1
CITED1	Hs00918448_m1
HOXB7	Hs04187556_m1
GDNF	Hs00181185_m1
FOXD1	Hs00270117_s1
PAX8	Hs00247586_m1
CHD16(KSP)	Hs00187880_m1
AQP1	Hs01028916_m1
ANEP(CD13)	Hs00174265_m1
CUBN	Hs00153607_m1
LRP2(Megalin)	Hs00189742_m1
CDH1(ECAD)	Hs01089742_m1
CDH2(NCAD)	Hs00983056_m1
WT1	Hs01103751_m1
SYNPO	Hs00200768_m1
NPHS1(Nephrin)	Hs00190446_m1
NPHS2(Podocin)	Hs00387817_m1
PODXL	Hs01574644_m1
CD2AP	Hs00961458_m1
GATA3	Hs00231122_m1
PECAM1	Hs01065279_m1
KDR1	Hs00911700_m1
GUSB	4326320E
B2M	4326319E
GAPDH	4326317E

Gene name	Common name	TaqMan assay ID
ABCC1	MRP1	Hs01561483_m1
ABCC2	MRP2	Hs00960489_m1
ABCC3	MRP3	Hs00978452_m1
ABCC4	MRP4	Hs00988721_m1
ABCC5	MRP5	Hs00981089_m1
ABCC6	MRP6	Hs01077866_m1
ABCB1	P-gp	Hs00184500_m1
ABCG2	BCRP	Hs01053790_m1
SLC15A1	PEPT1	Hs00192639_m1
SLC15A2	PEPT2	Hs01113665_m1
SLC22A2	OCT2	Hs01010726_m1
SLC22A4	OCTN1	Hs00268200_m1
SLC22A5	OCTN2	Hs00929869_m1
SLC22A6	OAT1	Hs00537914_m1
SLC22A7	OAT2	Hs00198527_m1
SLC22A8	OAT3	Hs00188599_m1
SLC22A11	OAT4	Hs00945829_m1
SLC22A12	URAT1	Hs01030727_m1
SLCO4C1	OATP4C1	Hs00698884_m1
SLC47A1	MATE1	Hs00217320_m1
SLC47A2	MATE2K	Hs00945650_m1
SLC31A1	CTR1	Hs00741015_m1
SLC34A1	NaPi2a	Hs00161828_m1
SLC34A3	NaPi2c	Hs02341449_m1

Supplemental table 2: Donor information for the adult, fetal, and control PTC samples used for comparison in the study.

Sample name	Company	Product number	Lot number	Gender	Age	Race
Adult kidney	Invitrogen	AM7979	1676404	Female	62	Hispanic
Fetal kidney	Clontech	636584	1412044	4 pooled; Male+Female	21-40 week	Asian
Control PTC-1	IVAL	HRPTC5105	-	Female	42	Caucasian
Control PTC-2	IVAL	HRPTC5108	-	Male	56	Caucasian
Control PTC-3	IVAL	HRPTC5109	-	Male	65	Caucasian

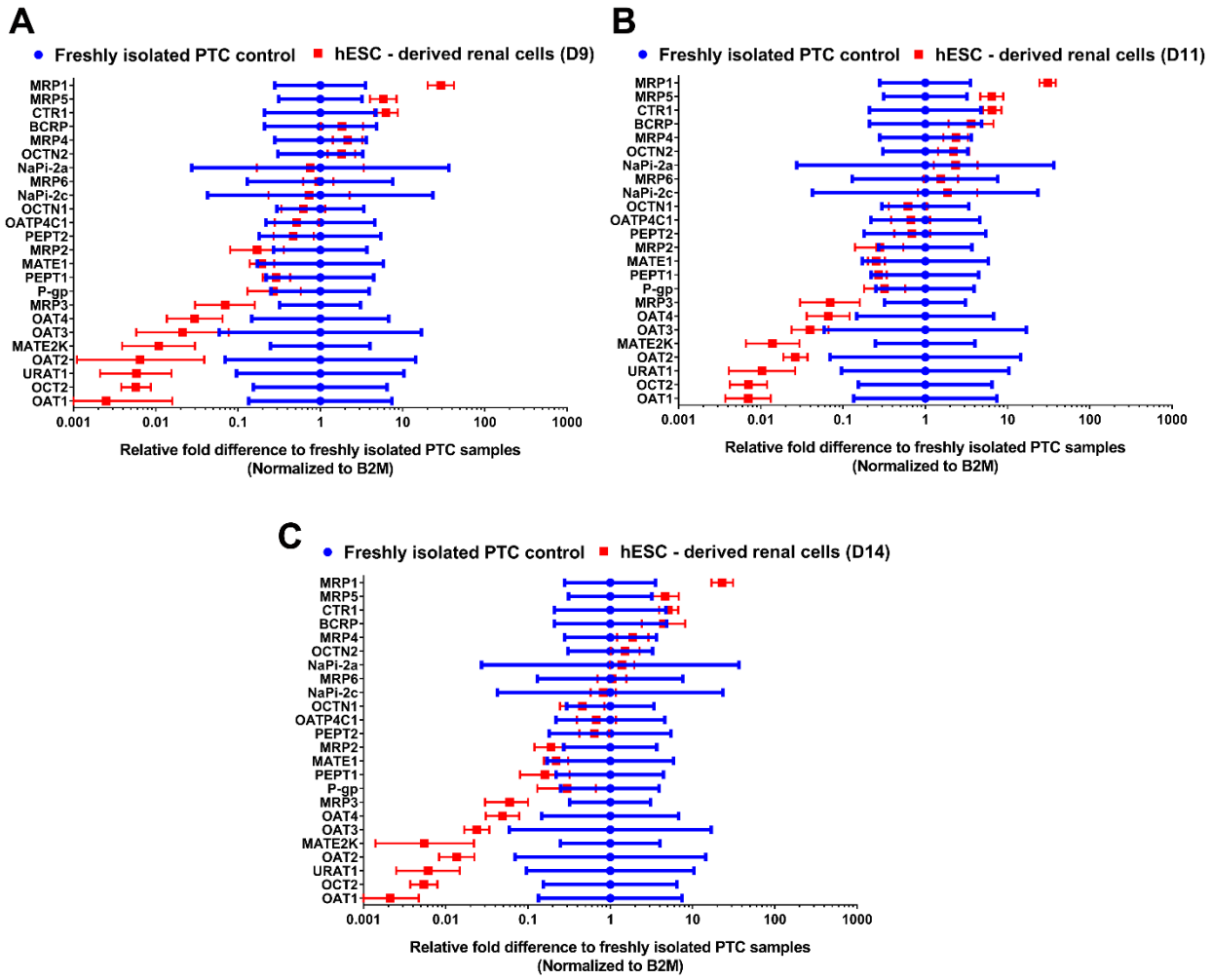

Supplementary Figure 1